NMR imaging and structure measurements using the long-range dipolar field in liquids

Chandrasekhar Ramanathan* and Richard W. Bowtell

Magnetic Resonance Centre, School of Physics and Astronomy, University of Nottingham, Nottingham NG7 2RD, United Kingdom

We extend the Fourier-based formalism previously developed to analyze structural measurements obtained using the long-range liquid dipolar field in NMR, in the short time regime. It is shown that in the case of a two-spin system, the signal measured in an average structure measurement is related to the spatial cross-correlation function of the spin densities of the two components. It is also demonstrated that in the case of cylindrically symmetrical systems, the measured data are related to the Meijer transform (or K transform) of the radial distribution function of the spin density. Experiments were performed on structured phantoms exhibiting cylindrical symmetry over the length scale probed, and were found to be in excellent agreement with the theory. Finally, it is shown that changes in image contrast with the strength of the modulation gradient can be expressed in terms of the action of a dipolar "filter."

INTRODUCTION

The use of NMR methods to obtain structural information has been well established since Mansfield and Grannell first showed NMR "diffraction" effects in solids [1] and later developed its relation to NMR imaging [2]. NMR diffusion measurements—in systems that restrict free diffusion—have been used to measure the autocorrelation of the shape function of a pore space [3], and this idea has been extended to NMR diffusive diffraction [4]. Barral *et al.* have also shown that the Fourier space data collected in a conventional NMR imaging experiment can yield the spatial autocorrelation function or Patterson function of the spin density of the system being studied [5]. Recently, average structure measurements have been obtained by exploiting the long-range dipolar field in liquids.

Long-range dipolar fields in liquids are not averaged out by molecular motions, and give rise to a resultant local field that is generally nonzero unless the system is spherically symmetrical [6]. This field has been ignored in most NMR experiments, but has recently become important with the shift to higher static magnetic fields. Numerous manifestations of this field have been observed—including the formation of multiple spin echoes in solid [7] and liquid ^{3}He [8], and water [9] in a two-pulse spin-echo experiment, dynamic line-shape distortions [10], and apparent intermolecular multiple-quantum coherences [11]. The dipolar field is generally nonlocal, with contributions to the field at each point coming from all positions in the sample. However, in the case of spatially modulated magnetization the dipolar field experienced by a spin is predominantly determined by the local magnetization located at a distance less than the wavelength of the modulation [11]. Since the modulation grating that is written onto the spins is under the control of the experimenter, it has been suggested that by manipulating the dipolar field it might be possible to extract structural infor-

mation about the sample [12]. This idea has been exploited in making structural measurements on systems containing a single spin species [13,14], and has been extended to systems with two different spin species located in different compartments within a sample [11,15–17].

Robyr and Bowtell showed that in an isotropic sample, the amplitude of the signal measured in the short time regime as a function of the gradient modulation is related to the Hankel transform of the radial distribution function [18]. In the present work, we ignore the effects of diffusion, but extend the formalism used to cylindrical structures as well as experiments on compartmentalized two-spin systems.

THEORY

Single spin species

Consider the standard n-quantum CRAZED (COSY-revamped by asymmetric z-gradients) pulse sequence illustrated in Fig. 1. In the following analysis, we neglect the effects of radiation damping, relaxation, and diffusion. Initially the entire sample magnetization is aligned along the external magnetic field $B_0\hat{z}$. When the magnetization is nutated, the dipolar field evolves with the magnetization. After a $(\pi/2)_y$ pulse, the magnetization is aligned along the x direction, and evolves under the first gradient pulse as $M_+(\vec{r}) = M_0(\vec{r})e^{i\vec{k}_m \cdot \vec{r}}$, where $|\vec{k}_m| = \gamma G \delta$, its direction is specified by the gradient direction, and $M_+ = M_x + iM_y$ as usual. After the θ pulse, we have

$$M_+(\vec{r}) = M_0(\vec{r})\left[\cos^2\left(\frac{\theta}{2}\right)e^{i\vec{k}_m \cdot \vec{r}} - \sin^2\left(\frac{\theta}{2}\right)e^{-i\vec{k}_m \cdot \vec{r}}\right] \quad (1)$$
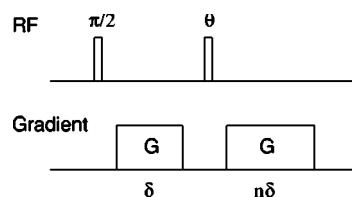

FIG. 1. The CRAZED experiment.

————
*Present address: Department of Nuclear Engineering, Massachusetts Institute of Technology, Cambridge, MA 02139; electronic address: sekhar@mit.edu

and

$$M_z(\vec{r}) = -M_0(\vec{r}) \frac{\sin\theta}{2} [e^{i\vec{k}_m \cdot \vec{r}} + e^{-i\vec{k}_m \cdot \vec{r}}]. \qquad (2)$$

After the second gradient pulse, M_z is unchanged, but M_+ becomes

$$M_+(\vec{r}) = M_0(\vec{r}) \left[\cos^2\left(\frac{\theta}{2}\right) e^{i(n+1)\vec{k}_m \cdot \vec{r}} - \sin^2\left(\frac{\theta}{2}\right) e^{i(n-1)\vec{k}_m \cdot \vec{r}} \right]. \qquad (3)$$

This magnetization evolves in the dipolar field according to the modified Bloch equations

$$\frac{dM_z}{dt} = -\frac{i\gamma}{2} [M_- B_{d+} - M_+ B_{d-}], \qquad (4)$$

$$\frac{dM_+}{dt} = -i\gamma [M_+ B_{dz} - M_z B_{d+}], \qquad (5)$$

where $\vec{B}_d$ is the dipolar field due to the spins ($B_{d+} = B_{dx} + iB_{dy}$; $B_{d-} = B_{dx} - iB_{dy}$). The dipolar field at a position $\vec{r}$ due to the magnetization of the sample is given by

$$\vec{B}_d(\vec{r}) = \frac{\mu_0}{4\pi} \int d^3\vec{r}' \frac{1 - 3\cos^2\theta_{rr'}}{2|\vec{r} - \vec{r}'|^3} [3M_z(\vec{r}')\hat{z} - \vec{M}(\vec{r}')]. \qquad (6)$$

The field is nonlocal and depends strongly on the shape of the sample. However, Deville *et al.* observed that this equation has the form of a convolution integral and showed that following a spatial Fourier transformation, the field becomes local in k space [7],

$$\vec{B}_d(\vec{k}) = \frac{\mu_0}{3} \Lambda(\hat{k})[3M_z(\vec{k})\hat{z} - \vec{M}(\vec{k})], \qquad (7)$$

where $\Lambda(\hat{k}) = \mathcal{P}_2(\hat{k} \cdot \hat{z})$ is the second-order Legendre polynomial of the cosine of the angle between $\hat{k}$ and the static magnetic field. The component $\vec{B}_d(\vec{k} = \vec{0})$ is the spatially uniform (dc) component of the magnetic field and is proportional to the total magnetization in the sample. The z component of this field can produce small, but observable shifts of the resonance frequency (for water protons at 500 MHz, $\gamma\mu_0 M_0 \approx 13$ rad/s).

The observed signal $S(\vec{k}_m, t)$ is obtained by integrating the transverse magnetization $M_+(\vec{r})$ over the entire sample. Defining $M_z^\Sigma = \int_{-\infty}^\infty d^3\vec{r} M_z(\vec{r})$ and $M^\Sigma = \int_{-\infty}^\infty d^3\vec{r} M_+(\vec{r})$, it can be shown that $dM_z^\Sigma/dt = 0$ and

$$\frac{dM^\Sigma}{dt} = -\frac{i\gamma\mu_0}{8\pi^3} \int_{-\infty}^\infty d^3\vec{k} \Lambda^*(\hat{k}) M_z^*(\vec{k}, t) M_+(\vec{k}, t), \qquad (8)$$

where $\Lambda^*(\hat{k}) = \Lambda(\hat{k}) = \mathcal{P}_2(\hat{k} \cdot \hat{z})$ [14]. At short times t after the second gradient pulse ($\gamma B_d t \ll 1$), the dipolar field only generates a small perturbation of the magnetization and

$M_z^*(\vec{k}, t)$ and $M_+(\vec{k}, t)$ can be replaced in Eq. (8) by their values at $t = 0$ yielding a linear growth of the signal with time,

$$S(\vec{k}_m, t) = -\frac{i\gamma\mu_0 t}{8\pi^3} \int_{-\infty}^\infty d^3\vec{k} \Lambda(\vec{k}) M_z^*(\vec{k}, 0) M_+(\vec{k}, 0). \qquad (9)$$

Taking the spatial Fourier transforms of Eqs. (2) and (3) and substituting them into Eq. (9), we get

$$S(\vec{k}_m, t) = \frac{i\gamma\mu_0 t \sin\theta}{16\pi^3} \int_{-\infty}^\infty d^3\vec{k} \Lambda(\hat{k})[M_0^*(\vec{k} - \vec{k}_m)$$
$$+ M_0^*(\vec{k} + \vec{k}_m)] \left[\cos^2\left(\frac{\theta}{2}\right) M_0(\vec{k} - (n+1)\vec{k}_m) \right.$$
$$\left. - \sin^2\left(\frac{\theta}{2}\right) M_0(\vec{k} - (n-1)\vec{k}_m) \right]. \qquad (10)$$

The integral in Eq. (10) depends on the relative magnitudes of the bandwidth (k_{max}) of $M_0(\vec{k})$ and the strength of the modulation $\vec{k}_m$. If $|\vec{k}_m|$ is smaller than k_{max}, the two terms in the first square brackets will overlap. The dipolar field is not well localized in this situation. For small values of n, the terms in the second square brackets overlap with those in the first, and a nonzero signal can be measured. In the absence of an external gradient modulation ($|\vec{k}_m| = 0$), the measured signal is proportional to $\int_{-\infty}^\infty d^3\vec{k} \Lambda(\hat{k})|M_0(\vec{k})|^2$, and is determined by the shape and structure of the sample.

In order to localize the dipolar field and avoid overlap between spectral components, the strength of the applied modulation must be at least k_{max}. When $|\vec{k}_m|$ is greater than k_{max}, the two terms in the first square brackets no longer overlap. This also ensures that each term in the second set of brackets can overlap with at most one term in the first set of brackets. In this case, the integral will reduce to zero unless $n = \pm 2$ or $n = 0$ (note that negative values of n correspond to cases in which the direction of the second gradient is reversed with respect to that of the first gradient). The results obtained in these three cases are, for $n = -2$,

$$S(\vec{k}_m, t) = \frac{i\gamma\mu_0 t \sin\theta \cos^2\left(\frac{\theta}{2}\right)}{16\pi^3} \int_{-\infty}^\infty d^3\vec{k} \Lambda(\vec{k} - \vec{k}_m)|M_0(\vec{k})|^2; \qquad (11)$$

for $n = 0$,

$$S(\vec{k}_m, t) = \frac{i\gamma\mu_0 t \sin\theta}{16\pi^3} \left[\cos^2\left(\frac{\theta}{2}\right) \int_{-\infty}^\infty d^3\vec{k} \Lambda(\vec{k} + \vec{k}_m) \left| M_0(\vec{k}) \right|^2 \right.$$
$$\left. - \sin^2\left(\frac{\theta}{2}\right) \int_{-\infty}^\infty d^3\vec{k} \Lambda(\vec{k} - \vec{k}_m) \left| M_0(\vec{k}) \right|^2 \right]; \qquad (12)$$
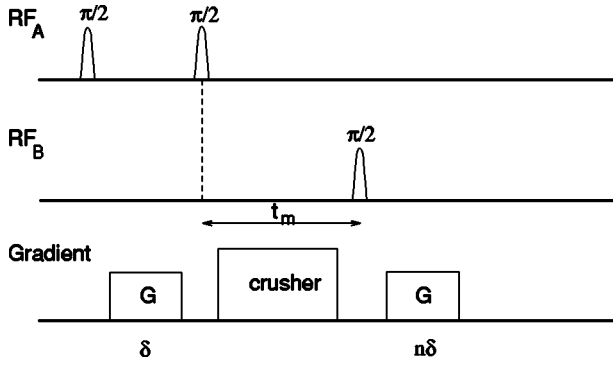
and for $n = 2$,

FIG. 2. The heteronuclear CRAZED experiment.

$$S(\vec{k}_m,t) = -\frac{i\gamma\mu_0 t \sin\theta \sin^2\left(\frac{\theta}{2}\right)}{16\pi^3}$$

$$\times \int_{-\infty}^{\infty} d^3\vec{k}\,\Lambda(\vec{k}+\vec{k}_m)|M_0(\vec{k})|^2. \qquad (13)$$

$|M_0(\vec{k})|^2$ has been shown to be the Fourier transform of the spatial autocorrelation function or the Patterson function $P_M(\vec{r})$ of the spin-density function [5]. Thus the NMR signal measured as a function of the modulation vector $\vec{k}_m$ is a convolution of the Fourier transform of the spin-density Patterson function and the dipolar weighting function $\Lambda(\vec{k})$.

Two spin species

Heteronuclear dipolar field experiments can be analyzed by considering the experiment shown in Fig. 2, where A and B are the two (different) spins in the sample [15–17].

The pulses used are now frequency-selective so that they only excite a single spin species. The first two $\pi/2$ pulses are tuned to the resonance of species A. The magnetization of spin species A after the second $\pi/2$ RF pulse is

$$M_+^A(\vec{r}) = iM_0^A(\vec{r})\sin(\vec{k}_m \cdot \vec{r}) \qquad (14)$$

and

$$M_z^A(\vec{r}) = -M_0^A(\vec{r})\cos(\vec{k}_m \cdot \vec{r}). \qquad (15)$$

The large gradient after the pulse crushes the transverse magnetization, $M_+^A(\vec{r})$. We assume that the interval t_m is short compared to the T_1 of species A, so that the modulated longitudinal magnetization remains locked unchanged along $\hat{z}$. Species B has not been perturbed by the first part of the experiment. The third $\pi/2$ RF pulse is a selective pulse tuned to the resonance of species B. After the modulation gradient pulse, the transverse magnetization is given by

$$M_+^B(\vec{r}) = M_0^B(\vec{r})e^{in\vec{k}_m \cdot \vec{r}}. \qquad (16)$$

The transverse magnetization of the B spins now evolves in the dipolar field created by the longitudinal magnetization of

the A spins. If $\omega_A - \omega_B \gg \gamma B_d$, the only effective term of the dipolar field is the component along $\hat{z}$, given by

$$B_{dz}^A(\vec{k}) = \frac{2\mu_0}{3}\Lambda(\hat{k})M_z^A(\vec{k})\hat{z}. \qquad (17)$$

The evolution of species B follows:

$$\frac{dM_+^B(\vec{r})}{dt} = -i\gamma_B M_+^B(\vec{r})B_{dz}^A(\vec{r}), \qquad (18)$$

yielding

$$M_+^B(\vec{r},t) = M_0^B(\vec{r})e^{in\vec{k}_m \cdot \vec{r}}\exp[-i\gamma_B B_{dz}^A(\vec{r})t]. \qquad (19)$$

At short times, we can expand the exponential to first order $(e^{-x} \approx 1-x)$, and get [19]

$$M_+^B(\vec{r},t) = M_0^B(\vec{r})e^{in\vec{k}_m \cdot \vec{r}}[1 - i\gamma_B B_{dz}^A(\vec{r})t]. \qquad (20)$$

Integrating the magnetization over the entire sample, we get the measured signal

$$S_B(\vec{k}_m,t) = \int_{-\infty}^{\infty} d^3\vec{r}[M_0^B(\vec{r})e^{in\vec{k}_m \cdot \vec{r}}$$
$$- i\gamma_B t M_0^B(\vec{r})e^{in\vec{k}_m \cdot \vec{r}}B_{dz}^A(\vec{r})]. \qquad (21)$$

The first integral reduces to zero under a strong gradient modulation. Considering the simplest case in which $n=1$, we apply Parseval's relations to get

$$S_B(\vec{k}_m,t) = -\frac{i\gamma_B t}{8\pi^3}\int_{-\infty}^{\infty} d^3\vec{k}[M_0^B(\vec{k}-\vec{k}_m)B_{dz}^{A*}(\vec{k})]. \quad (22)$$

Substituting the Fourier transform of Eq. (15),

$$S_B(\vec{k}_m,t) \approx \frac{i\mu_0\gamma_B t}{24\pi^3}\int_{-\infty}^{\infty} d^3\vec{k}\,\Lambda(\hat{k}+\hat{k}_m)M_0^B(\vec{k})M_0^{A*}(\vec{k}),$$
$$(23)$$

where we have again used the property that $\Lambda^*(\hat{k}) = \Lambda(\hat{k})$, and we have dropped the cross term $M_0^B(\vec{k}-\vec{k}_m)M_0^A(\vec{k}+\vec{k}_m)$. Comparing the result above with that obtained in the single-spin case [Eqs. (11)–(13)], it is seen that the signal obtained in this experiment as a function of $\vec{k}_m$ represents the Fourier transform of the cross correlation between the spin densities of the two components.

Average structure measurements

The results obtained in the above two cases can be cast in the general form $S(\vec{k}_m,t) = \mathcal{A}(\theta)\eta(\vec{k}_m)$, where $\mathcal{A}(\theta)$ contains the constants and angular factors and $\eta(\vec{k}_m)$ represents the integral over $\vec{k}$. Parseval's relation can then be used to evaluate $\eta(\vec{k}_m)$,

$$\eta(\vec{k}_m) = \int_{-\infty}^{+\infty} d^3\vec{k}\, \mathcal{C}(\vec{k})\Lambda(\vec{k}+\vec{k}_m) \tag{24}$$

$$= (8\pi^3)\int_{-\infty}^{+\infty} d^3\vec{r}\, \mathcal{P}(\vec{r})\Lambda(\vec{r})e^{-i\vec{k}_m\cdot\vec{r}}, \tag{25}$$

where

$$\Lambda(\vec{r}) = \frac{4\pi}{3}\frac{1-3(\hat{r}\cdot\hat{z})^2}{2|\vec{r}|^3} \tag{26}$$

and where $\mathcal{C}(\vec{k})$ represents either $|M_0(\vec{k})|^2$ or $M_0^B(\vec{k})M_0^{A*}(\vec{k})$ depending on the experiment, and $\mathcal{P}(\vec{r})$ represents the corresponding spatial auto- or cross-correlation function.

Thus, from Eq. (25), we see that the measured data correspond to the Fourier transform of the product of the spatial correlation function of the spin density and the weighting function $\Lambda(\vec{r})$, which can be considered to be a filter in real space. Considering the $n=+2$ case for a single spin species $[\mathcal{P}(\vec{r})=P_M(\vec{r})]$ as an illustrative example, the measured signal is

$$S(\vec{k}_m,t) = 8\pi^3\mathcal{A}(\theta)\int_{-\infty}^{+\infty} d^3\vec{r}\, P_M(\vec{r})\Lambda(\vec{r})e^{-i\vec{k}_m\cdot\vec{r}}. \tag{27}$$

Using the Fourier inversion formula, we can obtain the weighted Patterson function

$$P_M(\vec{r})\Lambda(\vec{r}) = \frac{1}{8\pi^3\mathcal{A}(\theta)}\int_{-\infty}^{+\infty} d^3\vec{k}_m S(\vec{k}_m,t)e^{+i\vec{k}_m\cdot\vec{r}}. \tag{28}$$

In order to obtain the three-dimensional Patterson function of a sample, we need to sample k space in all directions by repeating the experiment for different modulations and then apply the Fourier inversion procedure shown above. If the sample being studied has certain structural symmetries, the expressions in Eqs. (27) and (28) can, however, be simplified further. Note that while the spatial autocorrelation function of the spin density of a single spin species is used in the following discussion, it is equally applicable to the spatial cross-correlation function between the two spin species as shown above.

Spherical symmetry

For an isotropic medium, the Patterson function $P_M(\vec{r})$ depends only on the distance, r. We consider the direction of $\vec{k}_m$ to be fixed, and observe the signal as a function of its amplitude. Expanding Eq. (25) in spherical coordinates and integrating over the angular terms, we obtain

$$\eta(\vec{k}_m) = \frac{64\pi^4}{3}\Lambda(\hat{k})\int_0^\infty \frac{P_M(r)}{r}j_2(k_m r)dr, \tag{29}$$

where j_2 is a spherical Bessel function. The integration kernel $j_2(k_m r)$ describes the spatial variation of the dipolar field as a function of the modulation strength for the case of spherical symmetry [11,18]. By expanding the spherical Bessel function in terms of ordinary Bessel functions of fractional order, we can express $S(\vec{k}_m,t)$ in terms of a Hankel transform of the Patterson function of the spin density

$$S(\vec{k}_m,t) = \frac{i\sqrt{2}\pi^{1.5}\gamma\mu_0 t\sin\theta\sin^2\dfrac{\theta}{2}}{3\sqrt{k_m}}\Lambda(\hat{k})$$

$$\times\int_0^\infty \frac{P_M(r)}{r^{3/2}}J_{2.5}(k_m r)dr. \tag{30}$$

Note that $\Lambda(\hat{k})$ only depends on the angle between the direction of the applied external gradient and $\hat{z}$, and not on its magnitude. This term is maximal when the gradient is along $\hat{z}$ and zero at the magic angle. From the inversion formula for the Hankel transform [20], we get

$$\frac{P_M(r)}{r^{5/2}} = -\frac{3i}{\sqrt{2}\pi^{1.5}\gamma\mu_0 t\sin\theta\sin^2\dfrac{\theta}{2}}\left(\frac{1}{\Lambda(\hat{k})}\right)$$

$$\times\int_0^\infty S(k_m,t)J_{2.5}(k_m r)k_m^{3/2}\,dk_m, \tag{31}$$

which is the same as the expression obtained in [18], when diffusion effects are neglected. The Hankel transform also arises in other NMR experiments, such as pulsed field gradient measurements of spherically symmetric diffusion propagators [21], and in the imaging of spherically symmetric spin-density distributions [22].

Cylindrical symmetry

For long, oriented structures it is useful to consider the problem in cylindrical coordinates, where we assume that the sample extends infinitely along the axis of the cylinder and that the reduced Patterson function now depends only on the radial coordinate r in the cylindrical system. We can evaluate $\eta(\vec{k}_m)$ from Eq. (25) for a given direction of $\vec{k}_m$ using a cylindrical coordinate system aligned with the axis of our system, where this axis (w) is oriented at an angle α with respect to the static magnetic field,

$$\eta(\vec{k}_m) = \frac{32\pi^4}{3}\int_0^\infty P_M(r)r\,dr$$

$$\times\int_0^{2\pi}d\phi\int_{-\infty}^{+\infty}dw\left(\frac{1-3\cos^2\theta_{rz}}{2|\vec{r}|^3}\right)e^{-i\vec{k}_m\cdot\vec{r}} \tag{32}$$

$$= \frac{32\pi^4}{3}\int_0^\infty P_M(r)r\,dr\int_0^{2\pi}d\phi e^{-ik_\perp r\cos(\phi_k-\phi)}$$

$$\times\int_{-\infty}^{+\infty}dw\left(\frac{1-3\cos^2\theta_{rz}}{2|\vec{r}|^3}\right)e^{-ik_\parallel w}, \tag{33}$$

where $k_\perp$ is the projection of the gradient perpendicular to the axis of the system and $k_\parallel$ is the projection parallel to the axis, and ϕ_k is the angle between $k_\perp$ and the x axis of the cylinder. The resulting expression for $\eta(\vec{k}_m)$ is (details of the derivation are presented in Appendix A)

$$\eta(\vec{k}_m) = \frac{64\pi^5}{3}(1 - 3\cos^2\alpha)k_\parallel \int_0^\infty dr P_M(r) K_1(k_\parallel r) J_0(k_\perp r) + \frac{64\pi^5}{3}\cos^2\alpha k_\parallel^2 \int_0^\infty dr r P_M(r) K_2(k_\parallel r) J_0(k_\perp r)$$

$$- \frac{32\pi^4}{3}\sin^2\alpha k_\parallel^2 \int_0^\infty dr r P_M(r) K_2(k_\parallel r)\{\pi J_0(k_\perp r) - 2\pi J_2(k_\perp r)\cos 2\phi_k\}$$

$$+ \frac{64\pi^5}{3}\sin 2\alpha \cos\phi_k k_\parallel^2 \int_0^\infty dr r P_M(r) K_1(k_\parallel r) J_1(k_\perp r), \tag{34}$$

where $K_\nu(x)$ is a modified Bessel function. This expression simplifies considerably in the following cases. If the cylinder axis is parallel to B_0, α is set to zero in Eq. (34), and

$$\eta(\vec{k}_m) = (-2)\frac{64\pi^5}{3}k_\parallel \int_0^\infty dr P_M(r) K_1(k_\parallel r) J_0(k_\perp r)$$

$$+ \frac{64\pi^5}{3}k_\parallel^2 \int_0^\infty dr r P_M(r) K_2(k_\parallel r) J_0(k_\perp r), \tag{35}$$

which reduces to [23]

$$\eta(\vec{k}_m) = \frac{64\pi^5}{3}k_\parallel^2 \int_0^\infty dr r P_M(r) K_0(k_\parallel r) J_0(k_\perp t). \tag{36}$$

Further, if the gradient is applied along the cylinder axis as well, $k_\perp = 0$, $J_0(0) = 1$ and a further simplification results,

$$\eta(\vec{k}_m) = \frac{64\pi^5}{3}k_\parallel^2 \int_0^\infty dr r P_M(r) K_0(k_\parallel r), \tag{37}$$

which has the form of a zeroth-order Meijer transform [20] or K transform [24]. The modified Bessel function kernel $K_0(k_\parallel r)$ describes the localization of the dipolar field in this geometry and has been described by us previously [15]. The Meijer transform of order ν is defined as

$$g(y) = \mathcal{K}_\nu(f(x)) = \int_0^\infty f(x) K_\nu(xy)(xy)^{1/2} dx \tag{38}$$

and its inverse is

$$f(x) = \frac{1}{\pi i}\int_{c-i\infty}^{c+i\infty} g(y) I_\nu(xy)(xy)^{1/2} dy, \tag{39}$$

where c is chosen large enough so that all the poles lie to the left of the line of integration in the complex plane. Therefore,

$$\eta(\vec{k}_m) = \frac{64\pi^5}{3}k_\parallel^{3/2}\mathcal{K}(r^{1/2}P_M(r)) \tag{40}$$

and the measured signal in the $n = -2$ case is

$$S(k_\parallel, t) = \frac{i4\pi^2\gamma\mu_0 t \sin\theta \cos^2\dfrac{\theta}{2}}{3}k_\parallel^{3/2}\mathcal{K}(r^{1/2}P_M(r)). \tag{41}$$

Using the inversion formula, we obtain

$$r^{1/2}P_M(r) = \frac{3}{4\pi^3\gamma\mu_0 t \sin\theta \cos^2\dfrac{\theta}{2}}\int_{c-i\infty}^{c+i\infty} k_\parallel^{-3/2}S(k_\parallel, t) I_0(k_\parallel r)$$

$$\times(k_\parallel r)^{1/2}\ dk_\parallel. \tag{42}$$

It is necessary to perform a numerical inversion of the Meijer transform, since we only sample $k_\parallel$ on the real line (similar to a Laplace transform) [25]. References [20] and [24] provide tables of the inverse Meijer transforms of some known functions. We did not investigate the inversion of the Meijer transform in this paper. Equation (34) can also be expressed in terms of the Meijer transform.

Imaging

The formalism developed above can also be used to describe the changes observed in NMR images acquired using the CRAZED sequence, as a function of the applied modulation gradient. Starting from $S(\vec{k}_m, t) = \mathcal{A}(\theta)\eta(\vec{k}_m)$, we can use Parseval's relations to expand $\eta(\vec{k}_m)$,

$$\eta(\vec{k}_m) = \int_{-\infty}^{+\infty} d^3\vec{k}\,\Lambda(\vec{k} + \vec{k}_m)M_0^*(\vec{k})M_0(\vec{k}) \tag{43}$$

$$= (8\pi^3)\int_{-\infty}^{+\infty} d^3\vec{r}\,B_{dz}(\vec{r})M_0(\vec{r}), \tag{44}$$

where $B_{dz}(\vec{r})$ is the z component of the dipolar field in real space. Therefore, the signal measured in an imaging experiment is given by

$$S(\vec{k}_m, \vec{r}) = 8\pi^3 \mathcal{A}(\theta) B_{dz}(\vec{r}) M_0(\vec{r}) \qquad (45)$$

as long as the modulations of the imaging gradients and the dipolar field-selective gradients are well separated in magnitude. The image obtained is therefore a product of a spin-density image $M_0(\vec{r})$ and the dipolar field $B_{dz}(\vec{r})$. Thus it is the spatial variation of the dipolar field as a function of the applied modulation that explains the changes in the image contrast with the modulation [15]. Signal attenuation due to diffusion and flow in the modulation gradients and in local susceptibility gradients can also modulate the image contrast. The dipolar field in Fourier space is given by

$$B_{dz}(\vec{k}) = \Lambda(\vec{k} + \vec{k}_m) M_0(\vec{k}), \qquad (46)$$

where

$$\Lambda(\vec{k}) = \frac{1 - 3(\hat{k} \cdot \hat{z})^2}{2}. \qquad (47)$$

The k-space dipolar field can therefore be considered to be a product of the k-space spin density and a dipolar "filter" function $\Lambda(\vec{k})$. In the special case in which the system under study is cylindrically symmetrical (and appears infinite in z), $M(\vec{k}) = M(k_\rho)\delta(k_z)$. If, in addition, we now apply the modulation along the z direction, the k-space filter reduces to the following form:

$$\Lambda(\vec{k} + \vec{k}_m) = \Lambda(k_\rho, k_m) = \frac{1}{2} \frac{k_\rho^2 - 2k_m^2}{k_\rho^2 + k_m^2}. \qquad (48)$$

Thus a gradient applied along the z direction (along the cylinder axis) produces a radially varying filter function. This function varies smoothly from $-1/2$ for $k_m \ll k_\rho$ to $+1$ for $k_m \gg k_\rho$. Figure 6 shows the form of the filter for various values of k_m. For strong gradient modulations, $B_{dz}(\vec{r})$ is directly proportional to $M_0(\vec{r})$, and the image obtained is proportional to $M_0^2(\vec{r})$. This property has been used to spatially map the true spin density or water concentration in the human brain at 3 T, without using a calibration phantom [26].

EXPERIMENTAL RESULTS AND DISCUSSION

We performed experiments on samples of dimethylsiloxane (DMSO) at 298 K on a 11.7 T (500 MHz) homebuilt microimaging system [27], with an actively screened gradient coil set. The sample was placed in a 12-mm tube which was centered in a 16-mm-diam, 3.5-cm-long cylindrical birdcage RF coil. Two different structural phantoms were used, both containing sections of nylon string packed into the tube of DMSO. The diameter of the nylon string in the first phantom was 1.1 mm, while that in the second phantom was 0.7 mm. Figures 3(a) and 3(d) show images of the two phantoms, Figs. 3(b) and 3(e) show the corresponding spin-density Patterson functions, and Figs. 3(c) and 3(f) show the
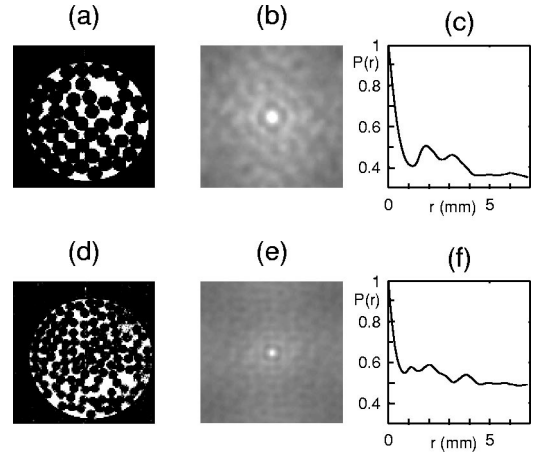

FIG. 3. (a) Image of phantom 1, (b) corresponding spin-density Patterson function, and (c) radial distribution function; (d) image of phantom 2, (e) corresponding spin-density Patterson function, and (f) radial distribution function.

radial distribution functions obtained from the image data [5]. It is seen that the first minimum of the function occurs at a distance which is close to the diameter of the nylon string used in each case as expected, as the filling factor is almost maximal in these phantoms.

The pulse sequence used is shown in Fig. 4. We used $n = -2$, which yields a maximum signal at $\theta = \pi/3$. The modulation gradients were applied along the z axis. The first (nonselective) π pulse was used to refocus static field inhomogeneities and allow the dipolar signal to grow [see Eq. (9)]. Crusher gradients were placed along the y axis on either side of the π pulse. The second π pulse is slice-selective for the imaging sequence. The echo time t_{E2} is relatively short in order to limit the time that the magnetization evolves under the action of a dipolar field that is modified by the effects of slice selection. A standard spin-warp imaging sequence was used for image acquisition. A four step $(x,y,-x,-y)$ phase cycle was applied to the first $\pi/2$ pulse along with a receiver phase cycle of $(x,-x,x,-x)$ to filter out the unwanted residual, conventional spin echo, and FID signals. 128×128 images were obtained with a field of view of 14 mm $\times$ 14 mm and gradient modulations k_m ranging from 0.55 mm^{-1} to 44 mm^{-1}. Four averages were acquired for the first phantom and a single average for the second phantom.
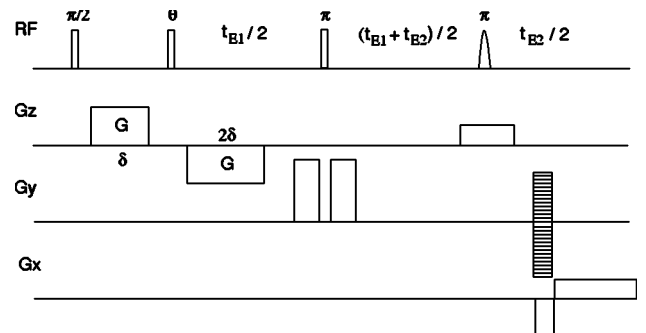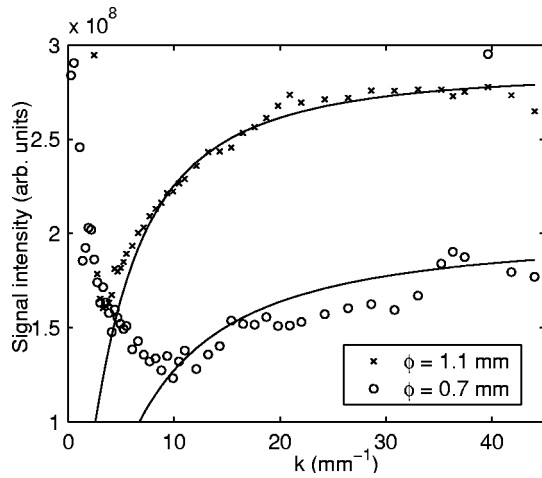

FIG. 4. Experimental pulse sequence.

FIG. 5. Integrated signal intensity as a function of the modulation strength for the two experimental phantoms used. The continuous lines are the best fit of Eq. (41) to the data in each case.

FIG. 6. Images of phantom 1, phantom 2, and the filter function given in Eq. (48), for gradient modulations $k_m = 6.1$ mm^{-1} [(a), (e), and (i)]; $k_m = 15.4$ mm^{-1} [(b), (f), and (j)]; $k_m = 30.8$ mm^{-1} [(c), (g), and (k)]; and $k_m = 41.8$ mm^{-1} [(d), (h), and (l)].

The time between the $\pi/2$ pulse and the $\pi/3$ pulse was 1.8 ms. t_{E1} was set to 62.88 ms, while t_{E2} was set to 30.68 ms. The duration of the first modulation gradient pulse was 1 ms and that of the second pulse was 2 ms. The T_1 of the DMSO was measured to be 2.42 s using an inversion recovery sequence. The pulse repetition time was set to 7 s. As the self-diffusion of DMSO is relatively slow ($D = 0.73 \times 10^{-9}$ m^2/s at 298 K [28]), diffusional attenuation is minimal over the time scale of the experiment and can be ignored.

The integrated signal intensities as a function of the modulation wave vector for the two phantoms are shown in Fig. 5, along with the corresponding simulation results. The simulations were performed by evaluating Eq. (41) as a function of k for the experimentally determined radial distribution functions of the two phantoms. As the spatial resolution of experimentally obtained RDFs is limited by the image resolution, we assumed that the radial distribution function was not changing rapidly between our sampled points and we used low pass interpolation to resample the function at a higher frequency. We found an optimal interpolation factor, such that resampling at a higher frequency did not change the integral obtained. The increased resolution was required in order to stabilize the evaluation of the Meijer transform, as the integral in the equation involves a zero multiplied by infinity near the origin. The evaluation of the Meijer transform was then performed on this resampled data set. A linear fit was then used to scale the numerical simulations and the experimental data. As can be seen from the figure, there is a significant discrepancy between the data and the simulations at low modulation strengths. This is the regime where there is significant overlap between the different terms in the first bracket of Eq. (10), and hence the analytical form of the Meijer transform is not valid. In addition, at small modulation strengths, the phase cycling was unable to completely suppress the large undesired signal due to the FID and the conventional spin echo. As the modulation strength
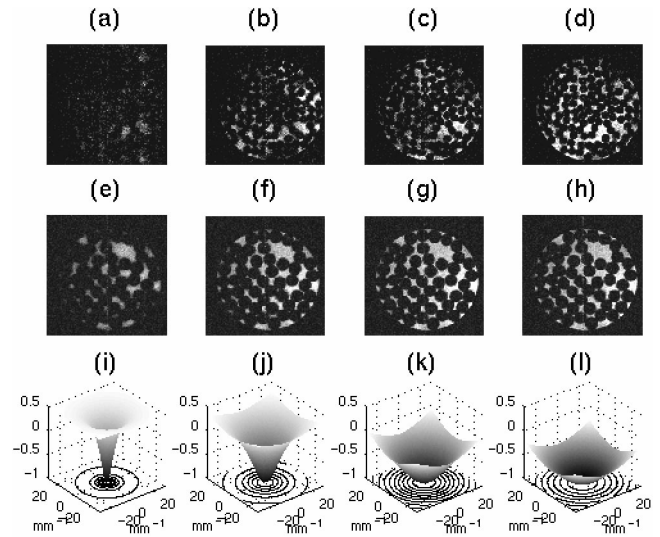
increases, it becomes easier to suppress the undesired signal.

Figure 6 shows the results of imaging experiments performed on both the phantoms as well as the resulting form of the filter in Eq. (48). It is seen that the image intensity and sharpness change significantly as the modulation is varied, becoming increasingly sharper and clearer with increasing gradient modulation. This is consistent with the further localization of the dipolar field at strong gradient modulations. The modulation strengths shown are $k_m = 6.1$ mm^{-1}, $k_m = 15.4$ mm^{-1}, $k_m = 30.8$ mm^{-1}, and $k_m = 41.8$ mm^{-1}. It is seen that changes in modulation produced with an axial gradient can significantly change the signal sensitivity to structural information in the radial direction.

CONCLUSIONS

In this paper we have extended the Fourier-based formalism developed earlier to study structural information using the long-range liquid dipolar field in NMR. This formalism provides a powerful framework within which to analyze dipolar field scattering measurements, and can be applied to average structure measurements in both single and multiphase spin systems, as well as to describe the changes in contrast produced in imaging experiments.

ACKNOWLEDGMENTS

APPENDIX

We start by writing Eq. (33) again,

$$\eta(\vec{k}_m) = \frac{32\pi^4}{3}\int_0^\infty P_M(r)rdr\int_0^{2\pi}d\phi\int_{-\infty}^{+\infty}dw\left(\frac{1-3\cos^2\theta_{rz}}{2|\vec{r}|^3}\right)e^{-i\vec{k}_m\cdot\vec{r}}$$

$$= \frac{32\pi^4}{3}\int_0^\infty P_M(r)rdr\int_0^{2\pi}d\phi\ e^{-ik_\perp r\cos(\phi_k-\phi)}\int_{-\infty}^{+\infty}dw\left(\frac{1-3\cos^2\theta_{rz}}{2|\vec{r}|^3}\right)e^{-ik_\parallel w}. \tag{A1}$$

Since

$$\cos^2\theta_{rz} = \frac{w^2\cos^2\alpha + r^2\sin^2\alpha\cos^2\phi + 2rw\cos\alpha\sin\alpha\cos\phi}{r^2+w^2}, \tag{A2}$$

we can express the last integral in Eq. (A1) as

$$I = \int_{-\infty}^{+\infty}dw\left[\frac{w^2(1-3\cos^2\alpha)+r^2(1-3\sin^2\alpha\cos^2\phi)-6rw\sin\alpha\cos\alpha\cos\phi}{2(r^2+w^2)^{5/2}}\right]e^{-ik_\parallel w}. \tag{A3}$$

Considering the even and odd properties of the different terms,

$$I = 2\int_0^\infty dw\left[\frac{w^2(1-3\cos^2\alpha)+r^2(1-3\sin^2\alpha\cos^2\phi)}{2(r^2+w^2)^{5/2}}\cos(k_\parallel w)+i\frac{6rw\sin\alpha\cos\alpha\cos\phi}{2(r^2+w^2)^{5/2}}\sin(k_\parallel w)\right]$$

$$= (1-3\cos^2\alpha)\int_0^\infty dw\frac{\cos(k_\parallel w)}{(r^2+w^2)^{3/2}}+3r^2[1-\sin^2\alpha(1+\cos^2\phi)]\int_0^\infty dw\frac{\cos(k_\parallel w)}{(r^2+w^2)^{5/2}}$$

$$+6ir\sin\alpha\cos\alpha\cos\phi\int_0^\infty dw\frac{w\sin(k_\parallel w)}{(r^2+w^2)^{5/2}}. \tag{A4}$$

The first two terms are Fourier cosine transforms and the third is a Fourier sine transform. These transforms are readily obtained from tables of integral transforms [24],

$$\mathcal{F}_C\left(\frac{x^{2m}}{(x^2+a^2)^{\nu+1/2}}\right) = \frac{(-1)^m a^{-\nu}\sqrt{\pi}}{2^\nu\Gamma(\nu+1/2)}\frac{d^{2m}}{dy^{2m}}[y^\nu K_\nu(ay)], \tag{A5}$$

$$\text{Re } a>0, 0\leq m<\text{Re }\nu+1/2,$$

$$\mathcal{F}_S\left(\frac{x^{2m+1}}{(x^2+a^2)^{n+1/2}}\right) = \frac{(-1)^{m+1}\sqrt{\pi}}{2^n a^n\Gamma(n+1/2)}\frac{d^{2m+1}}{dy^{2m+1}}[y^n K_n(ay)], \tag{A6}$$

$$\text{Re } a>0, -2\leq 2m<2n,$$

where K_ν is the modified Bessel function of order ν. Therefore, Eq. (A4) becomes

$$I = (1-3\cos^2\alpha)\frac{\sqrt{\pi}}{2r\Gamma(3/2)}k_\parallel K_1(k_\parallel r)+3[1-\sin^2\alpha(1+\cos^2\phi)]\frac{\sqrt{\pi}}{4\Gamma(5/2)}k_\parallel^2 K_2(k_\parallel r)$$

$$-6i\sin\alpha\cos\alpha\cos\phi\frac{\sqrt{\pi}}{4r\Gamma(5/2)}\frac{d}{dk_\parallel}[k_\parallel^2 K_2(k_\parallel r)] \tag{A7}$$

$$= (1-3\cos^2\alpha)\frac{k_\parallel}{r}K_1(k_\parallel r)+\cos^2\alpha k_\parallel^2 K_2(k_\parallel r)-\sin^2\alpha\cos^2\phi k_\parallel^2 K_2(k_\parallel r)+i\sin 2\alpha\cos\phi k_\parallel^2 K_1(k_\parallel r), \tag{A8}$$

where we have used $\Gamma(3/2)=0.5\Gamma(1/2)$ and $\Gamma(5/2)=0.75\Gamma(1/2)$ and $\Gamma(1/2)=\sqrt{\pi}$. The derivative in Eq. (A8) was evaluated using Ref. [23]. If we substitute Eq. (A8) into Eq. (A1), it can be seen that the integral over ϕ contains the following terms:

$$\int_0^{2\pi} d\phi\, e^{-ik_\perp r\cos(\phi_k-\phi)} = \int_0^{2\pi} d\phi \sum_{l=-\infty}^{+\infty} i^l J_l(-k_\perp r) e^{il(\phi_k-\phi)} = 2\pi J_0(k_\perp r), \tag{A9}$$

$$\int_0^{2\pi} d\phi \cos\phi\, e^{-ik_\perp r\cos(\phi_k-\phi)} = \int_0^{2\pi} d\phi \sum_{l=-\infty}^{+\infty} i^l J_l(-k_\perp r) e^{il(\phi_k-\phi)} \left(\frac{e^{i\phi}+e^{-i\phi}}{2}\right) = -2\pi i J_1(k_\perp r)\cos\phi_k, \tag{A10}$$

$$\int_0^{2\pi} d\phi \cos^2\phi\, e^{-ik_\perp r\cos(\phi_k-\phi)} = \int_0^{2\pi} d\phi \sum_{l=-\infty}^{+\infty} i^l J_l(-k_\perp r) e^{il(\phi_k-\phi)} \left(\frac{e^{2i\phi}+2+e^{-2i\phi}}{4}\right) = \pi J_0(k_\perp r) - 2\pi J_2(k_\perp r)\cos 2\phi_k. \tag{A11}$$

Therefore, substituting Eq. (A8) into Eq. (A1) and integrating over ϕ,

$$\eta(\vec{k}_m) = \frac{64\pi^5}{3}(1-3\cos^2\alpha)k_\parallel \int_0^\infty dr\, P_M(r) K_1(k_\parallel r) J_0(k_\perp r) + \frac{64\pi^5}{3}\cos^2\alpha k_\parallel^2 \int_0^\infty dr\, r P_M(r) K_2(k_\parallel r) J_0(k_\perp r)$$

$$- \frac{32\pi^4}{3}\sin^2\alpha k_\parallel^2 \int_0^\infty dr\, r P_M(r) K_2(k_\parallel r)\{\pi J_0(k_\perp r) - 2\pi J_2(k_\perp r)\cos 2\phi_k\}$$

$$+ \frac{64\pi^5}{3}\sin 2\alpha \cos\phi_k k_\parallel^2 \int_0^\infty dr\, r P_M(r) K_1(k_\parallel r) J_1(k_\perp r), \tag{A12}$$

which yields Eq. (34).

---

[1] P. Mansfield and P.K. Grannell, J. Phys. C **6**, 422 (1973).

[2] P. Mansfield and P.K. Grannel, Phys. Rev. B **12**, 3618 (1975).

[3] D.G. Cory and A.N. Garroway, Magn. Reson. Med. **14**, 435 (1990).

[4] P.T. Callaghan, A. Coy, D. MacGowan, K.J. Packer, and F.O. Zelaya, Nature (London) **351**, 467 (1991).

[5] G.A. Barral, L. Frydman, and G.C. Chingas, Science **255**, 714 (1992).

[6] A. Vlassenbroek, J. Jeener, and P. Broekaert, J. Mang. Reson. A **118**, 234 (1996).

[7] G. Deville, M. Bernier, and J.M. Delrieux, Phys. Rev. B **19**, 5666 (1979).

[8] D. Einzel, G. Eska, Y. Hirayoshi, T. Kopp, and P. Wölfle, Phys. Rev. Lett. **53**, 2312 (1984).

[9] R.W. Bowtell, R.M. Bowley, and P. Glover, J. Magn. Reson. (1969-1992) **88**, 643 (1990).

[10] H.T. Edzes, J. Magn. Reson. (1969-1992) **86**, 293 (1990).

[11] W.S. Warren, W. Richter, A.S. Andreotti, and B.T. Farmer III, Science **262**, 2005 (1993).

[12] W. Richter, S. Lee, W.S. Warren, and Q. He, Science **267**, 654 (1995).

[13] R.W. Bowtell and P. Robyr, Phys. Rev. Lett. **76**, 4971 (1996).

[14] P. Robyr and R.W. Bowtell, J. Chem. Phys. **106**, 467 (1997).

[15] R.W. Bowtell, S. Gutteridge, and C. Ramanathan, J. Magn. Reson. **150**, 147 (2001).

[16] S.M. Brown, P.N. Sen, and D.G. Cory, J. Chem. Phys. **116**, 295 (2002).

[17] S.M. Brown, P.N. Sen, and D.G. Cory, J. Magn. Reson. **154**, 154 (2002).

[18] P. Robyr and R.W. Bowtell, J. Chem. Phys. **107**, 702 (1997).

[19] We can analyze the experiment in the long time regime by integrating the magnetization over the entire sample, expanding the exponential in Eq. (19) as a Taylor series and applying Parseval's relations to get

$$S_B(\vec{k}_m,t) = \frac{1}{8\pi^3} \int_{-\infty}^\infty d^3\vec{k} \left[M_0^B(\vec{k}-n\vec{k}_m) \sum_{l=0}^\infty \frac{i^l \gamma_B^l t^l}{l!} (B_{dz}^{Al})^* \right], \tag{A13}$$

where

$$B_{dz}^{Al}(\vec{k}) = [B_{dz}^A(\vec{k}) \star B_{dz}^A(\vec{k}) \star \cdots \star B_{dz}^A(\vec{k})]_{l\text{times}}, \tag{A14}$$

$B_{dz}^A(\vec{k})$ is given in Eq. (17) above and $\star$ represents a convolution. Since $B_{dz}(\vec{k})$ is of the form of $M_0^A(\vec{k}-\vec{k}_m)+M_0^A(\vec{k}+\vec{k}_m)$, B_{dz}^{Al} will contain terms ranging from $M_0^A(\vec{k}-l\vec{k}_m)$ to $M_0^A(\vec{k}+l\vec{k}_m)$. Thus for a gradient of magnitude $|nk_m|$, the first nonzero term on the right-hand side of the above equation is $l=n$.

[20] V.A. Ditkin and A.P. Prudnikov, *Integral Transforms and Operational Calculus* (Pergamon Press, Oxford, 1965), English edition.

[21] S. Stapf, K.J. Packer, S. Békri, and P.M. Adler, Phys. Fluids **12**, 566 (2000).

[22] P.D. Majors and A. Caprihan, J. Magn. Reson. (1969-1992) **94**, 225 (1991).

[23] *Handbook of Mathematical Functions*, edited by M. Abramowitz and I.A. Stegun (Dover Publications, New York, 1972).

[24] H. Bateman, *Tables of Integral Transforms – Volumes I and II* (McGraw-Hill, New York, 1954).

[25] The Meijer transform is closely related to the Laplace transform, and reduces to it (apart from a scaling factor) for the special in which $\nu = \pm 1/2$ [24].

[26] S. Gutteridge, C. Ramanathan, and R.W. Bowtell, Magn. Reson. Med. **47**, 871 (2002).

[27] R.W. Bowtell, G.D. Brown, P.M. Glover, M. McJury, and P. Mansfield, Philos. Trans. R. Soc. London, Ser. A **333**, 457 (1990).

[28] M. Holz, S.R. Heil, and A. Sacco, Phys. Chem. Chem. Phys. **2**, 4740 (2000).